Journal of Statistical Mechanics: Theory and Experiment
An IOP and SISSA journal

Propagation of acoustic waves as a probe for distinguishing heterogeneous media with short-range and long-range correlations

S M Vaez Allaei[1,2], **Muhammad Sahimi**[3] and **M Reza Rahimi Tabar**[4,5]

[1] Department of Physics, University of Tehran, Tehran 14395-547, Iran
[2] Institute for Advanced Studies in Basic Sciences, Gava Zang, Zanjan 45195-1159, Iran
[3] Mork Family Department of Chemical Engineering and Materials Science, University of Southern California, Los Angeles, CA 90089-1211, USA
[4] Department of Physics, Sharif University of Technology, Tehran 11365-9161, Iran
[5] Institute of Physics, Carl von Ossietzky University, D-26111 Oldenburg, Germany
E-mail: smvaez@ut.ac.ir, moe@iran.usc.edu and mohammed.r.rahimi.tabar@uni-oldenburg.de

Received 17 December 2007
Accepted 2 March 2008
Published 27 March 2008

Online at stacks.iop.org/JSTAT/2008/P03016
doi:10.1088/1742-5468/2008/03/P03016

Abstract. The propagation of acoustic waves in strongly heterogeneous media is studied using direct numerical simulations. Two types of heterogeneous media are considered. In one type, the spatial distribution of the local elastic constants contain long-range correlations with a power law, nondecaying correlation function. The correlation length is, therefore, as large as the linear size of the system. In the second type of heterogeneous media the correlation length is decreased, up to the linear size of the blocks in the computational grid and, therefore, the distribution of the elastic constants is uncorrelated or white noise, but with the same mean and variance as that of the correlated media. We find that there are fundamental differences between wave propagation in the two types of heterogeneous media. In particular, the evolution of four distinct characteristics of the waves, namely, the amplitude of the coherent wavefront (CWF), its width, the spectral densities and the

1742-5468/08/P03016+28$30.00

scalogram (wavelet transformation of the waves' amplitudes at different scales and times), and the dispersion relations are completely different for uncorrelated and correlated media. Such differences point to wave propagation experiments that can detect important characteristics of the heterogeneities that a medium may contain, and help distinguish correlated disordered media from uncorrelated ones.

Keywords: heterogeneous materials (theory)

Contents

1. Introduction

The link between the static and dynamical properties of heterogeneous materials, ranging from composite solids to porous media, has been a problem of fundamental interest for decades. In a disordered solid material, for example, one is interested [1, 2] in the relation between the morphology—the shape, size, and the spatial distribution of the material's microscopic elements—and the dynamics of any process that takes place in the material at the macroscale, such as transport of electrical current or stress. Likewise, the relation between the morphology of a porous material and its flow, transport, and other dynamical properties have been studied for decades [3, 4]. Such relations are important in view of the fact that it is usually much easier to measure the macroscopic properties of disordered materials than characterizing with precision the spatial distribution of their microscopic heterogeneities. Thus, any macroscopic measurement that can shed light on the morphology of a material is valuable and important.

An important tool for obtaining information on the morphology and contents of inhomogeneous media has been the study of how waves—both acoustic and elastic—propagate in such media. For example, seismic wave propagation and reflection are

J. Stat. Mech. (2008) P03016

utilized [5] to not only estimate the hydrocarbon content of a potential oil field, but also the spatial distribution of its porosity, fractures, and faults. In addition, understanding wave propagation in heterogeneous media is fundamental to such important problems as predicting when earthquakes may occur, detecting underground nuclear explosions, and what happens on the seafloor. The same basic techniques are used in such diverse fields as materials science and medicine [5].

In this paper we study how acoustic waves propagate in an inhomogeneous medium. In particular, we study the relation between several characteristics of the waves, such as the decay of their amplitude, and the morphology of the inhomogeneous medium in which the waves propagate. The rate of the decay of the amplitude of a wave that undergoes multiple scattering strongly influences how far the wave propagates in the medium. The amplitude decay itself is a strong function of the heterogeneities and, in particular, the distribution of the medium's local elastic constants. In many heterogeneous media, such as rock, the elastic constants are not only broadly distributed—varying over many orders of magnitude—but also contain extended correlations. The problem that we study, in addition to its general importance, has been motivated by three recent developments.

(1) Recent analysis of extensive data for the speed of wave propagation in large-scale porous media (oil and gas reservoirs) provided evidence [6] that the distribution of the elastic moduli of such porous formations may follow a fractional Brownian motion, a self-affine stochastic distribution with long-range correlations that are characterized by a *nondecaying* power law correlation function (see below). Interpretation of the data for a wave propagation experiment in a large-scale heterogeneous medium, such as an oil reservoir, has traditionally been based either on representing the medium by a uniform system, or by a disordered one with *weak* heterogeneities [5]. Therefore, it is important to study how long-range correlations affect wave propagation, as it is well known that such correlations have a deep effect on other phenomena in heterogeneous media [1]–[4].

(2) Depending on the spatial distribution of the elastic moduli and the strength of the disorder, one may have *localized* acoustic waves in *any* dimensions, [7]–[9] including three-dimensional (3D) disordered media.

(3) There is a direct link between the static morphology of an inhomogeneous medium, characterized by a spatial distribution of the local elastic constants with long-range, nondecaying correlations, and the shape and roughness of a wavefront that propagates in the medium [10].

A major goal of this paper is to study the effect of the heterogeneities, represented by a spatial distribution of the local elastic constants, and their correlations on acoustic wave propagation. Another goal of the paper is to explore the possibility of the existence of a relation between the amplitude decay and the evolution of frequency attributes of acoustic waves that propagate in an inhomogeneous medium, and the spatial distribution of the medium's local elastic constants. In particular, we search for an indicator that distinguishes unambiguously acoustic wave propagation in a disordered medium from one in which there are long-range correlations between the local elastic constants, of the type that was recently revealed by the analysis of the experimental data [6].

J. Stat. Mech. (2008) P03016

Thus, two distinct classes of disorder are considered. In one, the spatial distribution of the local elastic constants is white noise or uncorrelated. In practice, there are at least short-range correlations (if not long-range ones) between the local properties of a heterogeneous medium. The limiting resolution of the model that we use to represent a heterogeneous medium is the linear size of the blocks in the computational grid. Thus, a medium in which the correlation length is the same as the linear size of the blocks in the computational grid may be considered as one without any correlations, and the medium can be considered as completely uncorrelated.

In the second class of disorder that we consider, the spatial distribution of the local elastic constants contains long-range correlations, characterized by a power law, nondecaying correlation function, similar to what was revealed by the recent analysis of the experimental data [6] for large-scale porous media. In this case, the correlation length is as large as the linear size of the system. We then decrease the correlation length (see below), up to the linear size of the blocks in the computational grid, in order to study its effect on wave propagation. The variance of the white noise distribution and that of the one with power law, nondecaying correlations are taken to be equal, so that any difference between the results obtained with the two types of media may be attributed to the correlation properties of the distributions.

While the theory of elasticity of materials has provided deep understanding of the propagation of acoustic and elastic waves in a homogeneous and continuous medium, the same is not true about heterogeneous materials and media of the type that we consider in this paper. For example, as mentioned above, the heterogeneities may give rise to localization of the waves [7]–[9]—much like localization of electrons in disordered materials [11]. They also affect the average speed of the waves' propagation and the way their amplitude decays. They may also strongly influence the instantaneous frequencies that seismic receivers record and, hence, may have important implications for the interpretation of seismic data.

The literature on wave propagation in heterogeneous media, and in particular in rock and other types of porous media, is very extensive [5, 12, 13]. The propagation of acoustic waves, as it relates to condensed matter physics, has previously been studied by several groups [14]–[16]. For example, Baluni and Willemsen [16] studied the problem in a one-dimensional (1D) stratified medium (see also below) that consisted of an array of alternating layers with random thicknesses. The characterization of laboratory-scale porous materials using acoustic waves was investigated by several groups [17]. Attention has also been focused on propagation of acoustic waves in *fluid-saturated* porous media [18]–[21]. However, the aforementioned studies [14]–[21] neither considered the type of heterogeneous media that we model in the present paper, nor studied the issues that we investigate (see also below).

The rest of this paper is organized as follows. We begin in section 2 by describing in detail the model of wave propagation that we use in this paper. Section 3 is devoted to the description of the numerical technique that we utilize to solve the governing equation for acoustic wave propagation. How the numerical results are analyzed and the wave propagation is characterized is described in section 4. The results are presented and analyzed in section 5, where we consider a variety of models of heterogeneous media, and show how the amplitude decay, frequency attributes, and the width of the main part of the wavefront are affected by the types of heterogeneities that we consider.

doi:10.1088/1742-5468/2008/03/P03016

J. Stat. Mech. (2008) P03016

2. The model

To study the propagation of acoustic waves in a disordered medium, we solve the following scalar wave equation [22],

$$\rho\frac{\partial^2}{\partial t^2}\psi(\mathbf{x},t) - \boldsymbol{\nabla}\cdot[K(\mathbf{x})\boldsymbol{\nabla}\psi(\mathbf{x},t)] = 0, \tag{1}$$

where $K(\mathbf{x})$ and $\rho(\mathbf{x})$ are, respectively, the (analog of the) bulk modulus and the density of the medium at point $\mathbf{x}$. In sufficiently heterogeneous media, both $K(\mathbf{x})$ and $\rho(\mathbf{x})$ vary spatially. In this paper, we assume that the density is constant. Equation (1) represents the propagation of the waves in a system with *off-diagonal* disorder. In general, $\psi(\mathbf{x},t)$ represents the wave field. We restrict our attention to two-dimensional (2D) media, in which case equation (1) describes the transverse displacement in the system with varying tension K and constant mass density, or anti-plane shear in a 2D heterogeneous solid [22]. In the numerical simulations described below $K(\mathbf{x})$ is distributed according to a probability density function $f[K]$.

As mentioned in section 1, we consider two types correlation for spatial distribution $f[K(\mathbf{x})]$. In one, the correlation is taken to be a fractional Browning motion (FBM), consistent with the results of recent analysis of the data for large-scale porous media that indicated [6] that the FBM-type distributions describe, at least approximately, the spatial distribution of $K(\mathbf{x})$. The correlation function $C(r) = \langle[K(\mathbf{x}) - K(\mathbf{x}+\mathbf{r})]^2\rangle_x$ of an FBM is given by $C(r) \sim r^{2H}$, a nondecaying power law for all physically acceptable (positive) values of H. A convenient representation of an FBM is through its power spectrum—the Fourier transform of $C(r)$ of the spatial distribution of $K(\mathbf{x})$—which, for a d-dimensional FBM, is given by [23]

$$S(\boldsymbol{\omega}) = \frac{a_d}{(\sum_i \omega_i^2)^{H+d/2}}, \tag{2}$$

where a_d is a d-dependent constant, and $\boldsymbol{\omega} = (\omega_1, \ldots, \omega_d)$, with ω_i being the Fourier component in the ith direction. Here, $0 \leq H \leq 1$ is the Hurst exponent such that $H > 1/2 (< 1/2)$ implies positive (negative) correlations among the increments of the values generated by an FBM, while $H = 1/2$ is the usual Brownian case.

It has been suggested in the past [24] that reasonable models of rock can be obtained with a Hurst exponent $-1/2 < H < 0$, implying a heterogeneous medium in which the variation of $K(\mathbf{x})$ *decreases* with increasing scales. However, recent examination of the data [6] for large-scale porous media (oil reservoirs) indicates that $0 < H < 1$, i.e., the variance of $K(\mathbf{x})$ *increases* with increasing scales. This is the model that we utilize in this paper.

Very recently (after completion of our work), Pride and Masson [25] studied numerically the acoustic attenuation in fluid-saturated porous materials with an FBM distribution of the local elastic constants with $-2 < H < 2$. They showed that the waves' quality factor Q, where Q^{-1} is proportional to the acoustic attenuation, is given by $Q \propto \omega^{\chi}$ (ω is the frequency), with $\chi = \tanh H$. However, aside from utilizing an FBM distribution, the quantities that Pride and Masson [25] studied are unrelated to what we investigate in the present paper and previous ones [7, 8, 10].

J. Stat. Mech. (2008) P03016

Also studied is acoustic wave propagation in heterogeneous media in which the correlations are lost beyond a cutoff length scale ℓ. At the same time, almost all large-scale natural porous media that are of interest in geophysics are anisotropic, with the anisotropy being due to stratification (different layers of contrasting properties). To study acoustic wave propagation in both types of heterogeneous media, we modify the spectral representation of the FBM by introducing a cutoff length scale, $\ell = 1/\omega_c$, such that

$$S(\boldsymbol{\omega}) = \frac{b_d}{(\omega_c^2 + \sum_i \eta_i \omega_i^2)^{H+d/2}}, \tag{3}$$

where b_d is another d-dependent constant. The cutoff scale ℓ is such that for length scales $L < \ell$ values of $K(\mathbf{x})$ preserve their correlations ($H > 1/2$) or anticorrelations ($H < 1/2$), but for $L > \ell$ they become uncorrelated. Here, η_i is a parameter that generates stratification (layering) along the ith direction (for $\eta_i = 1$ we recover the isotropic distribution). Increasing η_i also increases the anisotropy in the sense of generating a larger number of layers. To distribute $K(\mathbf{x})$ according to an FBM we used the successive random addition method [26] for isotropic media, and the fast Fourier transform method [27] for anisotropic media.

If the cutoff scale ℓ is equal to the linear size of the blocks in the computational grid that we utilize in the numerical simulations, then we obtain the second type of heterogeneous media—one in which the spatial distribution of K is uncorrelated and white noise, but has the same mean and variance as those of the FBM distributions. We have set several distinct values to the mean (variance) of K, such as 0.7 (0.04), in our simulations.

3. Numerical simulation

Equation (1) is solved in two dimensions with up to 80 000 time steps, using the finite-difference (FD) method with second- and fourth-order discretization in the time and spatial domains, respectively. Thus, in discretized form, $\psi(\mathbf{x}, t)$ is written as $\psi_{i,j}^{(n)}$, where n denotes the time step number. The second-order FD approximation (accurate to Δt^2) to the time-dependent term of equation (1) is the standard form,

$$\frac{\partial^2 \psi(\mathbf{x}, t)}{\partial t^2} \simeq \frac{\psi_{i,j}^{(n+1)} - \psi_{i,j}^{(n)} + \psi_{i,j}^{(n-1)}}{\Delta t^2}, \tag{4}$$

where Δt is the time step's size. The time step for all cases was $\Delta t = 10^{-3}$. As for the spatial derivatives, we first expand the right-hand side of equation (1) as

$$\begin{aligned} \boldsymbol{\nabla} \cdot [K(\mathbf{x}) \boldsymbol{\nabla} \psi(\mathbf{x}, t)] &= \boldsymbol{\nabla} K(\mathbf{x}) \cdot \boldsymbol{\nabla} \psi(\mathbf{x}, t) + K(\mathbf{x}) \boldsymbol{\nabla}^2 \psi(\mathbf{x}, t) \\ &= \partial_x K(\mathbf{x}) \partial_x \psi(\mathbf{x}, t) + \partial_y K(\mathbf{x}) \partial_y \psi(\mathbf{x}, t) \\ &\quad + K(\mathbf{x}) \left[\partial_x^2 \psi(\mathbf{x}, t) + \partial_y^2 \psi(\mathbf{x}, t) \right]. \end{aligned}$$

Then, using the fourth-order FD discretization, we obtain, for example, for the derivatives in the x-direction,

$$\partial_x^2 \psi(\mathbf{x}, t) \simeq \frac{-\psi_{i+2,j}^{(n)} + 16\psi_{i+1,j}^{(n)} - 30\psi_{i,j}^{(n)} + 16\psi_{i-1,j}^{(n)} - \psi_{i-2,j}^{(n)}}{12\Delta x^2}, \tag{5}$$

J. Stat. Mech. (2008) P03016

and

$$\partial_x \psi(\mathbf{x}, t) \simeq \frac{-\psi^{(n)}_{i+2,j} + 8\psi^{(n)}_{i+1,j} - 8\psi^{(n)}_{i-1,j} + \psi^{(n)}_{i-2,j}}{12\Delta x}, \tag{6}$$

where Δx is the spacing between two neighboring grid points in the x direction. Similar expressions are written down for the partial derivatives with respect to the y direction. Such approximations proved to be accurate enough and provided the required stability to the numerical results, as we work in the limit of low frequencies, or wavelengths that are much larger than the linear size of the blocks of the computational grid.

Preliminary simulations were carried out using $L_x \times L_y$ grids to determine a large-enough size for the grid. Based on such simulations we used $L_x = 400$ and $L_y = 4000$ and 8000 (L_x and L_y are in units of the individual blocks in the computational grid). The main direction of wave propagation was taken to be the y direction (see figure 1(b)), while periodic boundary conditions were imposed in the x direction which, due to the large sizes of the computational grid, did not distort the nature of the wave propagation. The solution's accuracy was checked by considering its stability and the source's wavelength [28].

To investigate the wave propagation and its evolution in large grids, we insert a wave source at every node of the grid's first row at $y = 0$, which ensures the generation of a smooth initial wavefront. Using a point source will not change the results that we present below, although it would require a larger number of realizations to obtain reliable statistics. As the source function $S_0(t)$, we used the following to generate the pulse waves (any other source may also be used),

$$S_0(t) = -A(t - t_0) \exp[-\zeta(t - t_0)^2], \tag{7}$$

where A is a constant and ζ controls the waves' wavelength, which controls their width. To compute the amplitude decay and the frequency dependence of the waves during their propagation, we collect the numerical results at receivers (grid points) that are distributed evenly throughout the grid (see figure 1(b)), along the main direction of the wave propagation. Our simulations indicated that averaging the results over 85 realizations of the system suffices for obtaining results that will not change if we use a larger number of realizations. Figure 2 compares the averages for two different number of realizations, indicating their convergence to the true representative values.

4. Analysis of the numerical results and characterization of propagating waves

Figure 1(a) shows the shape and cycle of the wave at the source (at $y = 0$) that propagates throughout the heterogeneous medium. As the waves propagate in the medium, their multiple scattering generates many cycles of seemingly irregular oscillations. Such irregularities disappear for the averaged wave, i.e., one that represents an average over all the realizations. This is shown in figure 3, which compares the results for some of the realizations with those for the averaged wave. The first one of such cycles of the oscillations, or the first few of them—often called the *coherent wavefront* [29]—is an important characteristic of a propagating wave. An alternative definition of the coherent wavefront is that it is that part of the wave that remains intact after averaging over all the realizations. The value of ψ_c for the first peak (in the coherent front) and the time

J. Stat. Mech. (2008) P03016

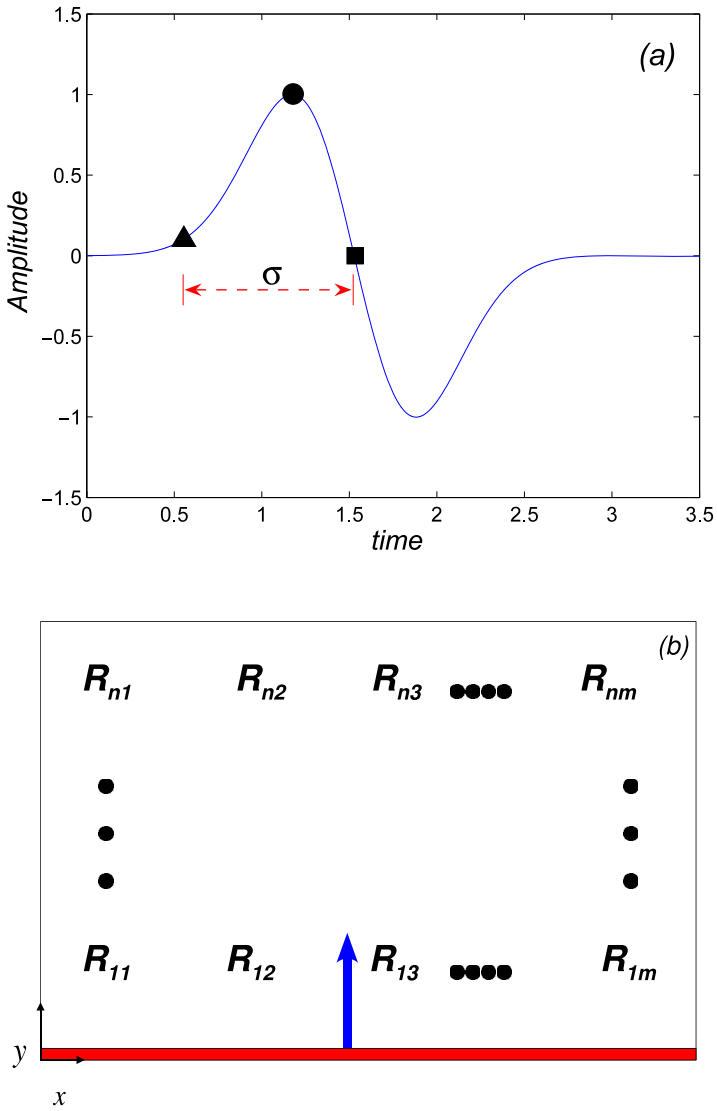

Figure 1. (a) The shape of the wave at the source. Triangles, circles, and squares denote, respectively, the time at which the amplitude is 10% of its peak value (shown by the circle), the peak position, and the first zero-crossing. σ is the width of the coherent wavefront. (b) The distribution of the receivers. The source is at the bottom of the system at $y = 0$. The arrow indicates the main direction of wave propagation.

(location) at which it occurs are also important characteristics of the propagation process. During the waves' propagation, the numerical value of ψ_c for the coherent wavefront decreases, while the front's width σ increases. Thus, we also focus on the decay of ψ_c and the shape of the coherent front, as characterized by σ. We show below that they generate distinct 'signatures' that contain information on the spatial distribution of $K(\mathbf{x})$. To do so, we measure the time dependence of ψ_c at a fixed distance from the source. Then, as we show below, from a sequence of measurements (collection of the numerical data) at every receiver, a qualitative picture of the evolution of the coherent wavefront versus the receivers' distance from the source emerges.

J. Stat. Mech. (2008) P03016

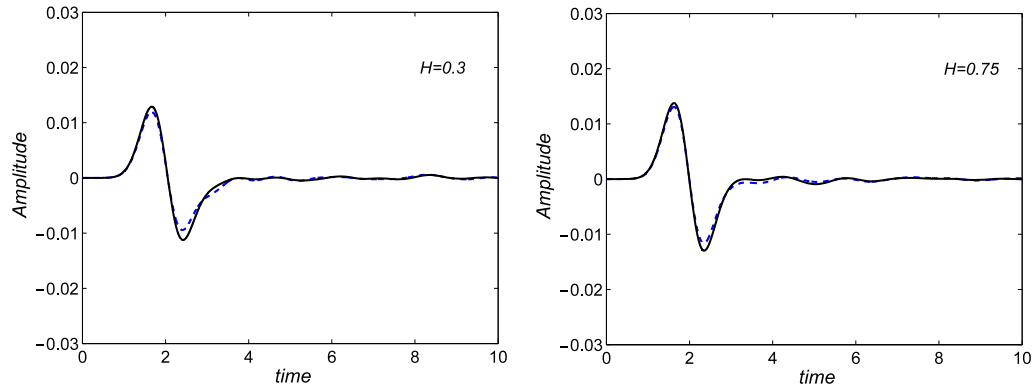

Figure 2. Comparison of the averaged ψ for 40 (dashed curve) and 60 (continuous curve) realizations.

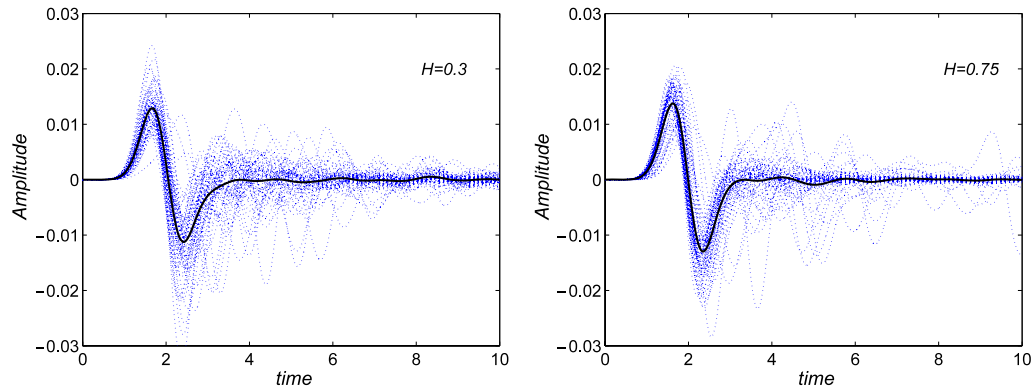

Figure 3. Comparison of the averaged ψ (dark continuous curves) with individual realizations.

Thus, to study quantitatively the evolution of the coherent wavefront, we characterize it by three properties: its peak value ψ_c; the time at which ψ attains 10% of the peak value ψ_c (the 10% is rather arbitrary, and only represents a rough measure of where the wave field becomes relatively significant); and its *first zero-crossing*—the time at which $\psi(\mathbf{x}, t)$ vanishes for the *first time* after the first peak. Then, the width σ of the coherent wavefront is defined as the time between the first zero-crossing and when the coherent wave's $\psi(\mathbf{x}, t)$ is 10% of the peak value ψ_c. These are all shown in figure 1(a). We show below that the manner by which these properties evolve depends strongly on the spatial distribution of $K(\mathbf{x})$. As they can be measured in practice, they provide important information on the spatial distribution of $K(\mathbf{x})$.

To characterize more precisely the propagation of acoustic waves, we need a tool that enables us to obtain the frequency content of the time series $\psi(\mathbf{x}, t)$—a process often referred to as the time–frequency analysis. The goal of such analysis is to expand the time series into the sum of wavelike forms, the time–frequency properties of which are adapted to the time series' local structure. The continuous wavelet transform

doi:10.1088/1742-5468/2008/03/P03016

J. Stat. Mech. (2008) P03016

(CWT) of a time series $s(u)$ is one such tool, which is defined by the following integral transform [30],

$$\hat{s}(\lambda, t) = \int_{-\infty}^{\infty} s(u)\bar{\Psi}_{\lambda,t}(u)\,\mathrm{d}u, \tag{8}$$

where

$$\Psi_{\lambda,t}(u) = \frac{1}{\sqrt{\lambda}}\Psi\left(\frac{u-t}{\lambda}\right) \tag{9}$$

represents a family of functions, referred to as the wavelets [30]. Here, λ is a scale parameter, t is a time (location) parameter representing the translation of the wavelet at different times, and $\bar{\Psi}$ is the complex conjugate of Ψ. $\Psi(u)$ is often referred to as the *mother wavelet*. Clearly, changing λ has the effect of dilating ($\lambda > 1$) or contracting ($\lambda < 1$) the function $s(u)$. On the other hand, varying t has the effect of analyzing the function $s(u)$ around different points at times t. When λ increases, the wavelet becomes more spread out and takes only the long-time behavior of $s(u)$ into account, and vice versa. Therefore, the WT provides a flexible timescale window that narrows when focusing on small-scale features, and widens on large-scale features. Note that $\Psi_{\lambda,t}(u)$ has the same shape for all values of λ.

The WT, as defined by equation (8), is a continuous transformation because the scale and time parameters, λ and t, assume continuous values. In our analysis we use the continuous complex Morlet wavelet [31], which is well known in geophysical applications [32], in order to obtain information about the instantaneous frequency attributes of the propagating waves, and to determine which part of the waves is scattered more during the propagation. The Morlet wavelet is given by

$$\Psi(t) = \pi^{-1/4}\exp[-(\mathrm{i}\omega_0 t - t^2/2)], \qquad \omega_0 \geq 5. \tag{10}$$

Since the Morlet wavelet is a complex function, it enables one to extract information about both the amplitude and phase of the process being analyzed. As an example, we show in figure 4 the CWT of $S_0(t)$ (using the Morlet wavelet), the source function given by equation (7). The vertical axis represents the scale λ, which is set to $\lambda = 2T_s$, where $T_s = 1/\nu_s$, with T_s and ν_s being the mean period and frequency, respectively. The horizontal axis is the dimensionless time, while the colors show the intensity of $|\hat{S}_0|^2(\lambda, t)$ at different times and scales. Using such plots—usually called the *scalogram* [32]—we determine the positions of the frequency modes on the time axis (i.e., the time at which they arrive at a given receiver) and, hence, determine which frequency attributes move faster than the others, and how the heterogeneities in the medium affect them.

We also compute the dispersion relations for the propagation of the waves in both correlated and uncorrelated media, [33], i.e., the relation between the angular frequency ω and the wavevector k ($k = 2\pi/\chi$, where χ is the wavelength). $\omega(k)$ characterizes the wave attenuation in a system, which we shall show to be very different for uncorrelated media (or those with short-range correlations) and those with long-range correlations, hence providing another signature of such correlations in a heterogeneous medium.

J. Stat. Mech. (2008) P03016

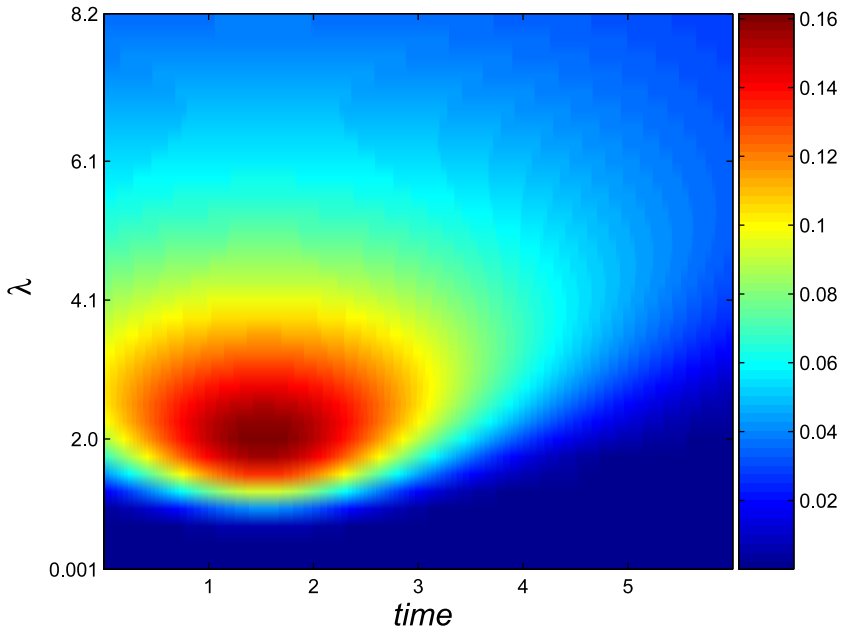

Figure 4. Scalogram (wavelet transform) of the source function $S_0(t)$, given by equation (8).

5. Results and discussion

One may characterize the propagation of waves in disordered media by the evolution of five key properties: (i) the decay in the value of $\psi_c(\mathbf{x}, t)$ of the coherent wavefront; (ii) the corresponding increase in the width σ of the coherent wavefront; (iii) the frequency attributes of the propagating waves, quantified by the power spectrum and the scalogram; (iv) the dispersion relation [34] for the propagation of the waves, a quantity that has been used extensively in the past for characterizing the phenomenon; and (v) the shape and roughness of the wavefront. Our focus in this paper is on the first four properties; the shape and roughness of wavefronts have been studied elsewhere [10, 35].

As pointed out above, as the acoustic waves propagate through a heterogeneous medium, the magnitude ψ_c of the first peak in the coherent front decreases with t, while the width σ of the front (as defined above) increases. The waves undergo multiple scattering, caused by the medium's heterogeneities, and strongly influence the evolution of such characteristics. In addition, the waves' passage through different zones of a heterogeneous medium with widely varying elastic constants, and the fact that the waves may be pinned [10, 35] in certain locations in the medium, also cause roughening of the wavefront, amplitude decay, and strong changes in the waves' frequency contents. The dispersion relation is also strongly affected by the correlation of $K(\mathbf{x})$. We have carried out direct numerical simulations, using several distinct models of heterogeneous media, to study acoustic wave propagation and, in particular, the evolution of the four key properties described above. In what follows we present and discuss the results.

J. Stat. Mech. (2008) P03016

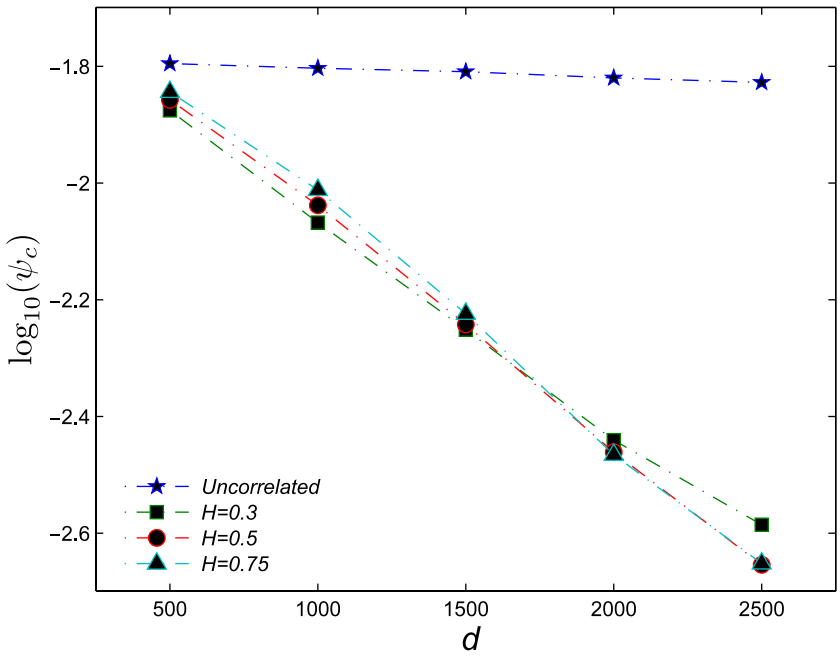

Figure 5. Dependence of the coherent wave amplitude ψ_c (the first peak in the plot of $\psi(\mathbf{x}, t)$ versus time) on the distance d between the source and the receivers. The local elastic constants are distributed according to an FBM with the Hurst exponent H. The medium is isotropic.

5.1. Isotropic media: long-range versus short-range correlations

As the first example, we consider acoustic wave propagation in a medium in which $K(\mathbf{x})$ has FBM correlation, and compare the results with those for an uncorrelated medium, but with the same mean and variance of the local elastic constants as those of the FBM. In an uncorrelated medium (one with short-range correlations, such that the correlation length is the same as the linear size of the blocks in the computational grid), the quantity ψ_c of the coherent wavefront decays as a power law in the distance d between the source and the receiver [36], at least if the distribution of $K(\mathbf{x})$ is not extremely broad. The same is true [29] about wave propagation in granular materials which represent unconsolidated porous media. However, the decay of ψ_c in a heterogeneous medium with long-range correlations is much faster, and takes on an exponential form—similar to electron localization. Thus, the exponential decay of ψ_c of the coherent wavefront is the first 'signature' of the existence of long-range correlations in a disordered medium, and in particular the nondecaying correlations that are generated by the FBM. Figure 5 confirms the exponential decay of the amplitude ψ_c in three heterogeneous media, and compares them with that in an uncorrelated medium but with the same mean and variance as in the FBM media.

Another feature of wave propagation is the broadening of the width σ of the coherent wavefront during the propagation. In uncorrelated media, the width of the coherent part increases with d as a power law [29], where d is the distance between the source and the receivers. However, in correlated media in which $K(\mathbf{x})$ is distributed according

J. Stat. Mech. (2008) P03016

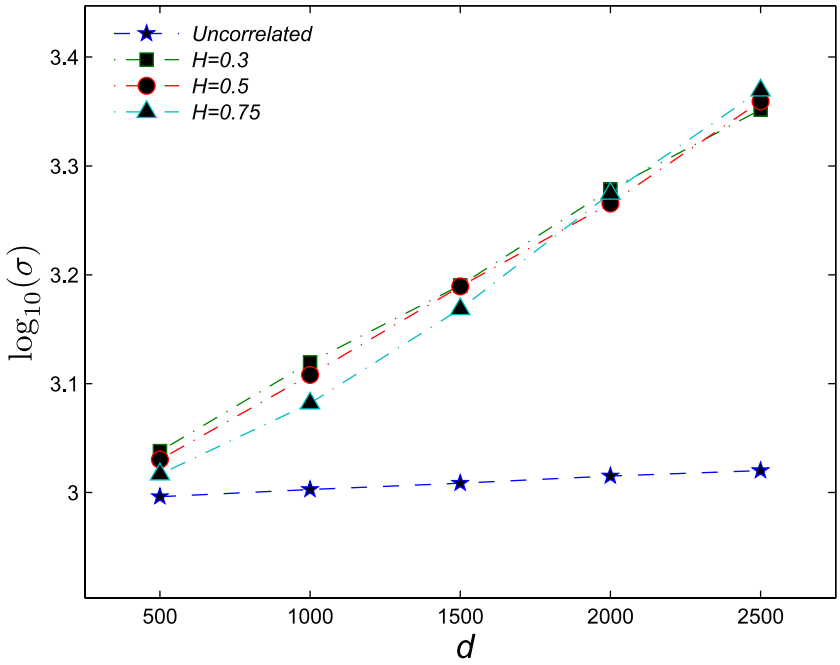

Figure 6. Dependence of the width σ of the coherent wavefront on the distance d between the source and the receivers, in an uncorrelated medium, as well as in an isotropic medium in which the local elastic constants are distributed according to an FBM with a Hurst exponent H.

to an FBM, the dependence of the width σ of the coherent wavefront on the source–receiver distance d is *exponential*, fundamentally different from that of uncorrelated media. This distinguishing feature between uncorrelated and correlated media is demonstrated in figure 6, where we present the width of the coherent wavefront for both types of heterogeneous media. Thus, the exponential dependence of the width σ of the coherent wavefront may be considered as the second signature of long-range correlations in heterogeneous media.

The third important feature of the waves is the frequency dependence of their power spectrum during the propagation. It is well known that in an uncorrelated medium the high-frequency modes scatter more efficiently than the low-frequency ones. Figure 7 presents the (normalized) spectral density of the waves that were received by four different sets of receivers located along the propagation direction (receivers R_{1i}–R_{4i} shown in figure 1(b)). The results, computed for the first few cycles of the amplitudes, represent averages over many realizations. As figure 7 indicates, the shape of the power spectrum changes when one computes or measures it at various receivers (various distances) throughout the medium in which the waves are propagating. As shown clearly, the ratio of low-frequency and high-frequency modes increases as the source–receiver distance d increases, hence indicating that, in *uncorrelated media*, the waves lose their high-frequency modes faster than the low-frequency ones.

In the correlated media that we consider, the evolution of the power spectrum is, however, different. Figure 8 presents the (normalized) spectral densities for $H = 0.3$ and 0.75 for the same receivers. The changes in all the spectral densities for each frequency is

J. Stat. Mech. (2008) P03016

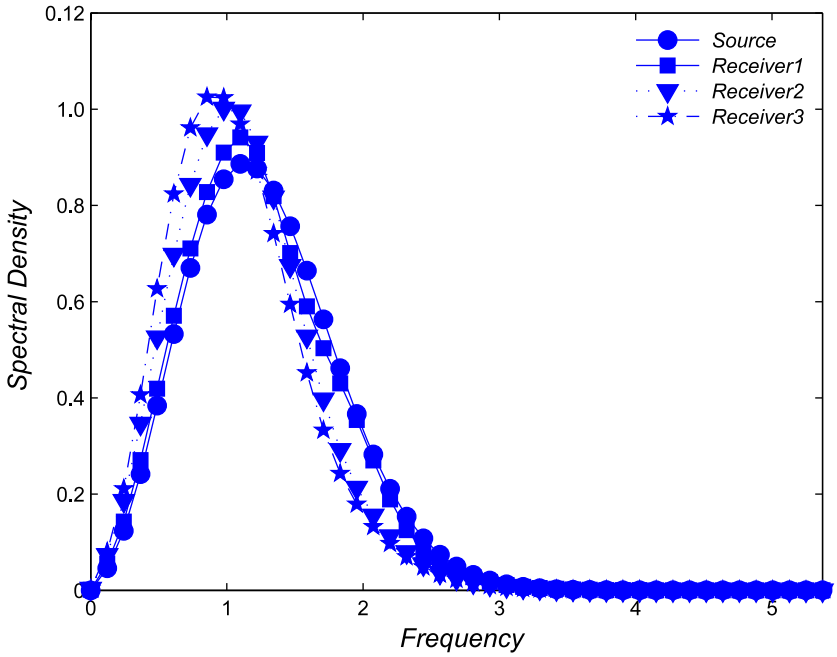

Figure 7. Normalized spectral density of the wavefront at the source, and at three different receivers located along the y direction (the main direction of wave propagation), in an uncorrelated medium.

approximately the same as for all other frequencies. Thus, when long-range correlations are present in the distribution of the local elastic constants, the low-frequency modes can be scattered just as efficiently and quickly as the high-frequency ones. This difference between the two types of spectral density may also be considered as evidence of long-range correlations in a disordered medium.

To make the distinction between the uncorrelated and correlated media clearer, we have computed the scalogram (the CWT of the first few cycles of the amplitude) of the waves arriving at various receivers, in order to determine their instantaneous frequency distribution during the propagation. Figure 4 presented the scalogram of the source wave used in the simulations. Figure 9 presents the scalogram of the wavefront received by four distinct receivers along the y direction (the main direction for wave propagation), namely, R_{12}, R_{22}, R_{32}, and R_{42}, from top to bottom, respectively. The different colors show the intensity of $|\hat{\psi}|^2(\lambda, t)$. In the top scalogram, the intensity in most of the diagram for $3 < t < 10$ is essentially zero (no wave has arrived there yet). But, in the scalogram at the bottom, which is for the waves that have arrived at the farthermost receiver, nonzero intensities appear in the same region. As seen clearly, especially for receivers R_{32} and R_{42} for times $t > 1$, after the main part there are some zones with nonzero intensity. Such zones indicate that the main parts of the waves lose some of their high-frequency attributes and, therefore, the lost frequencies arrive at the receiver(s) after a delay. This is consistent with what is presented in figure 7 for the spectral density of the same waves.

However, the scalogram for the case of an FBM distribution of the local elastic constants is completely different. Figures 10 and 11 show, respectively, the scalogram for the same receivers with the Hurst exponent $H = 0.3$ and 0.75. The features of the

J. Stat. Mech. (2008) P03016

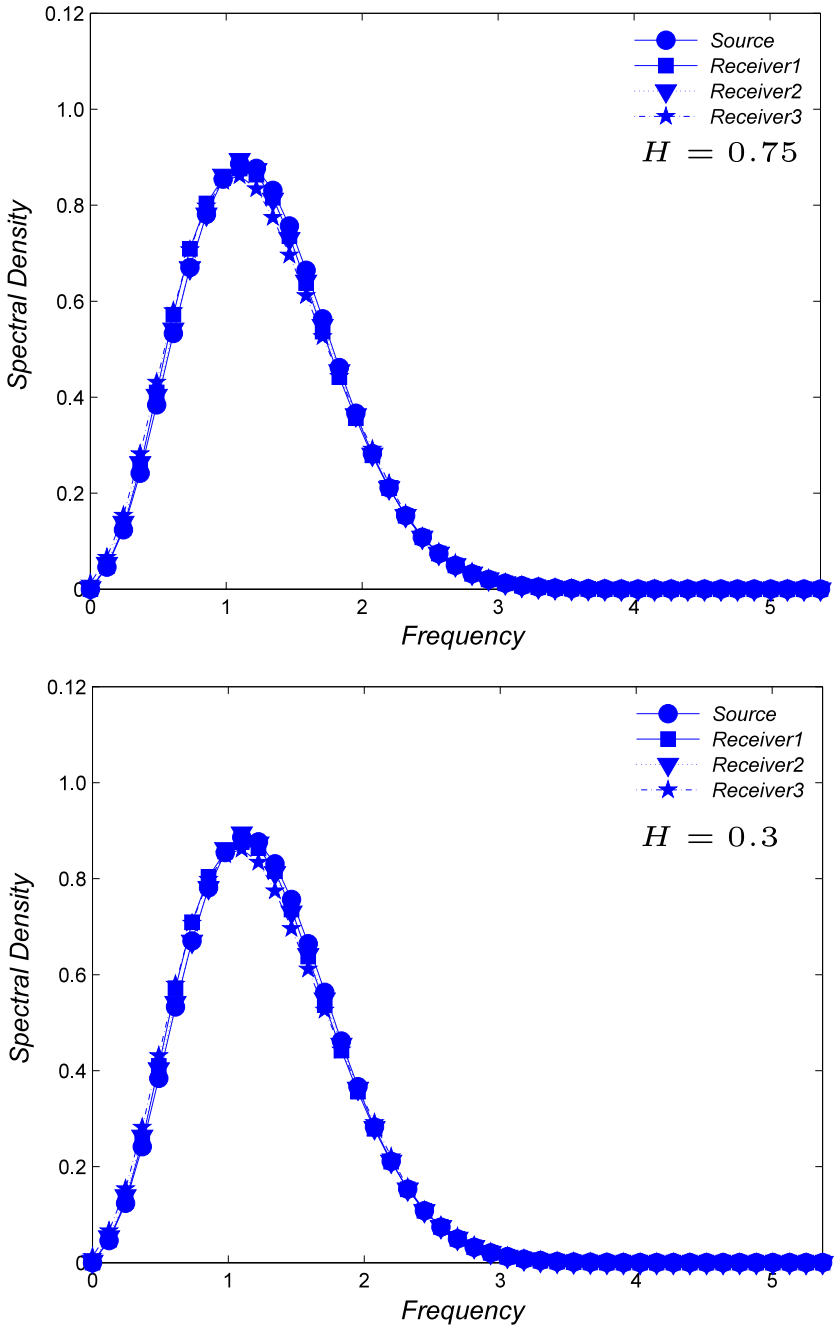

Figure 8. Same as in figure 7, but in isotropic correlated media with a Hurst exponent H.

evolution of these scalograms are in sharp contrast with those shown in figure 9. *All* the receivers receive *all* the frequencies after the main part of the wave, hence indicating that essentially *simultaneous* scattering of all the frequency modes is one major feature of wave propagation in heterogeneous media in which the spatial distribution of the local elastic constants contains long-range correlations. This important difference between the scalograms of uncorrelated and correlated media, which can be computed rather

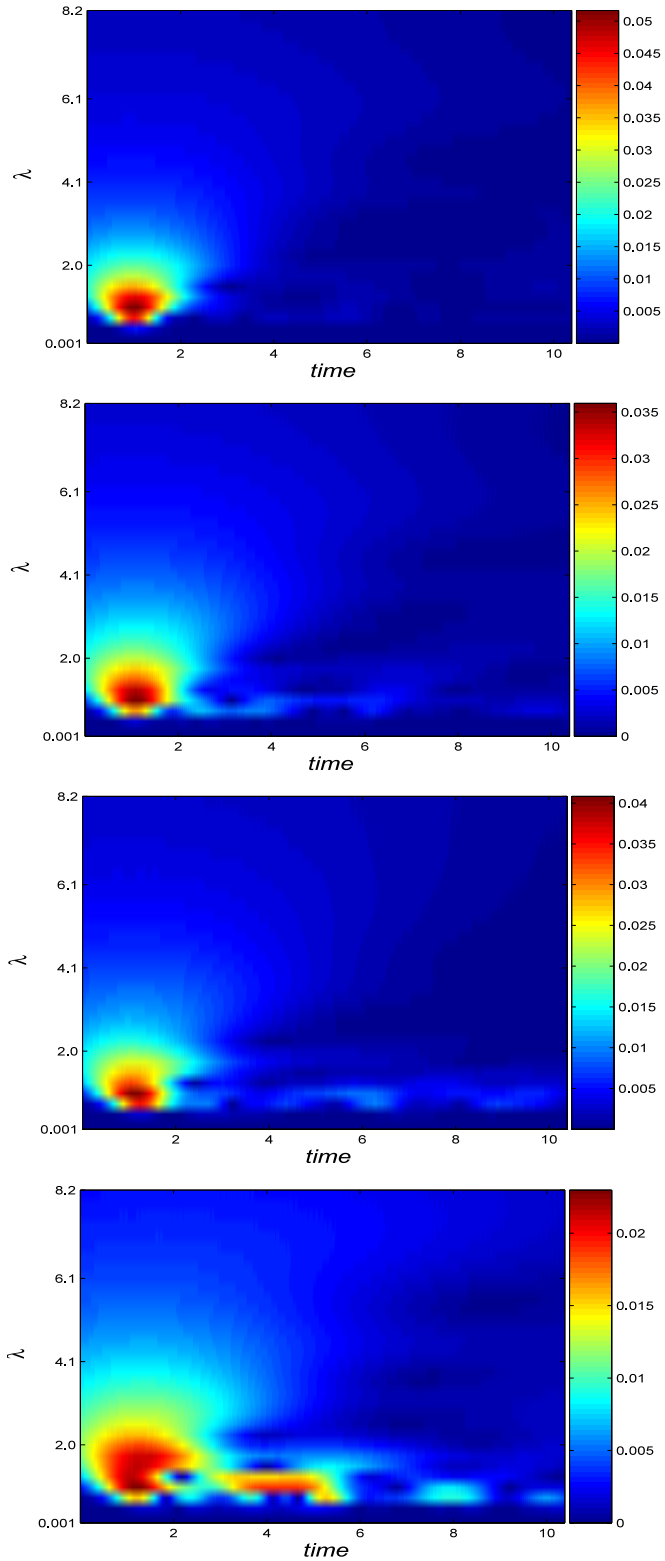

Figure 9. Scalogram (wavelet transform) of the wavefront, received by four different receivers, located along the direction of wave propagation, in an uncorrelated medium. The diagrams show, from top to bottom, the results for the receivers closest to, and farthermost from, the source.

J. Stat. Mech. (2008) P03016

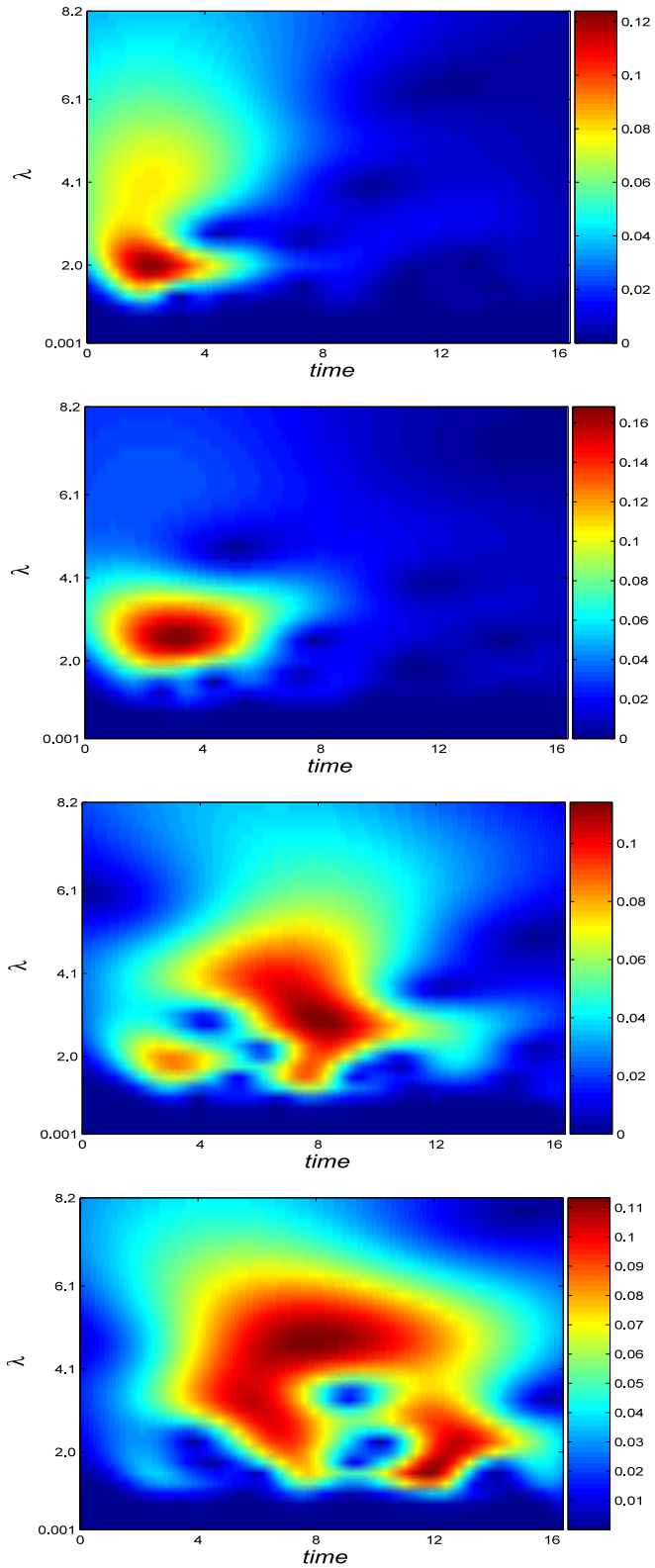

Figure 10. Same as in figure 9, but for an isotropic correlated medium with an FBM distribution of the local elastic constants with the Hurst exponent $H = 0.3$.

J. Stat. Mech. (2008) P03016

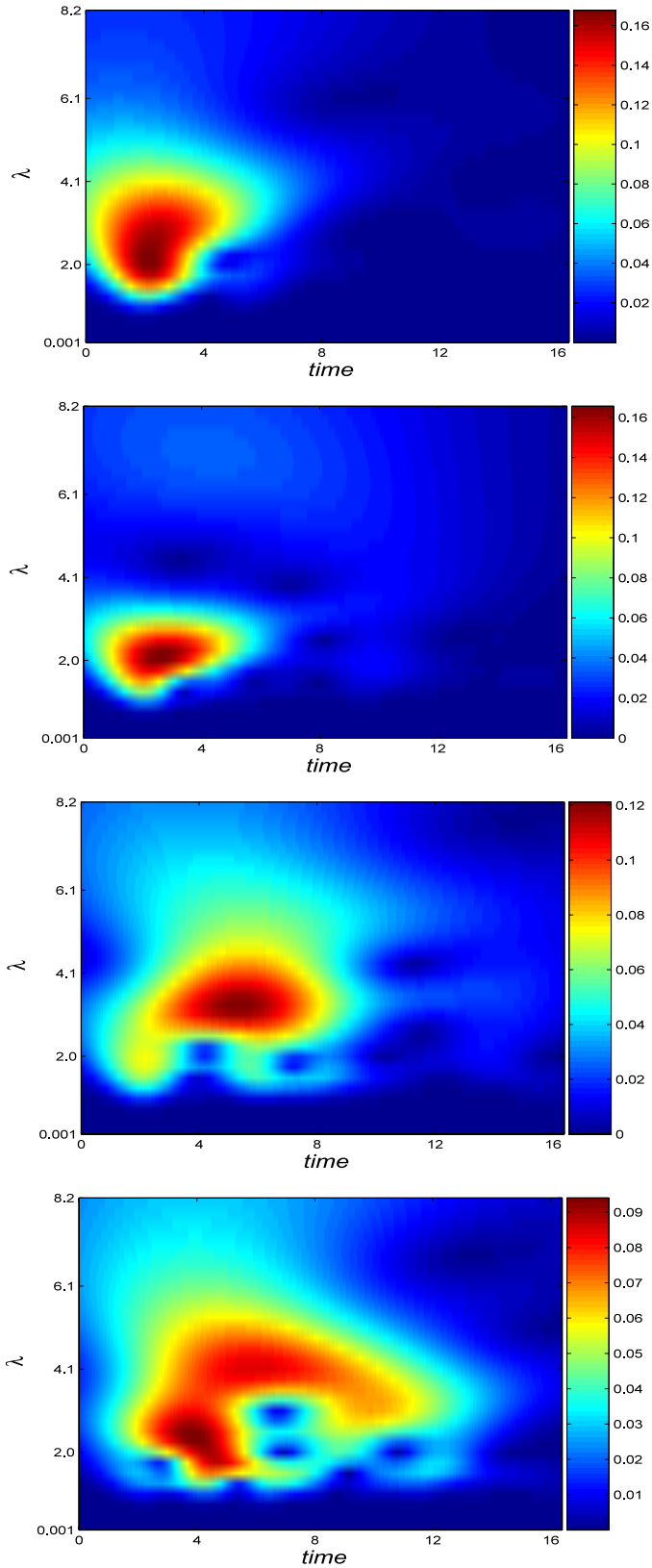

Figure 11. Same as in figure 10, but with the Hurst exponent $H = 0.75$.

J. Stat. Mech. (2008) P03016

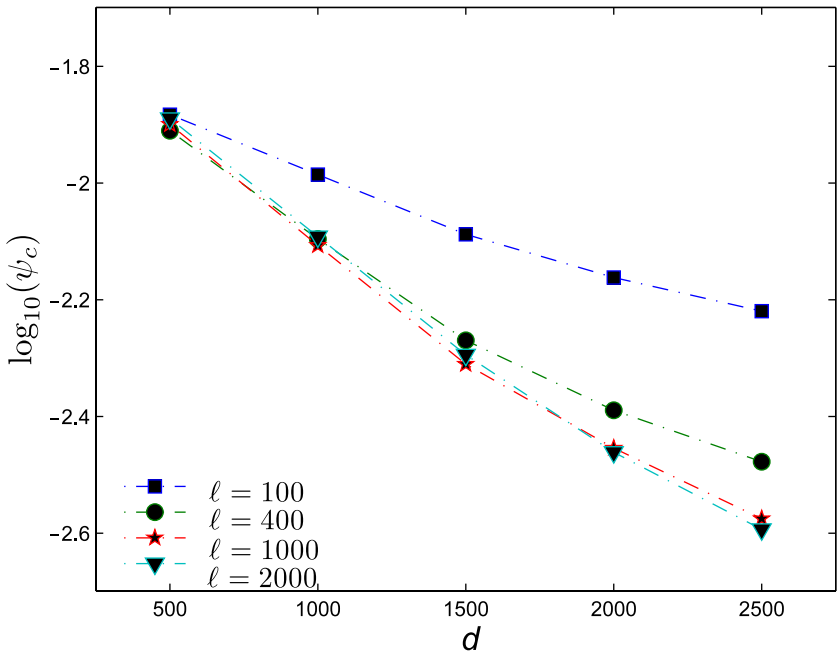

Figure 12. The decay of the amplitude ψ_c of the coherent part of the wave with the distance d between the source and the receivers. The results are for an isotropic medium with an FBM correlation of the local elastic constants and a Hurst exponent $H = 0.3$. ℓ is the cutoff length for the correlations in the distribution of the local elastic constants.

straightforwardly in practical applications of wave propagation (for example, for seismic exploration data, or for seismic data emanated from an earthquake hypocenter), may also be considered as another 'signature' of the existence of such correlations in the local elastic moduli. Note also the differences between the scalograms in figures 10 and 11 for positive (persistent, $H > 0.5$) and negative (antipersistent, $H < 0.5$) correlations.

5.2. The effect of a cutoff in the correlations

The distinction between uncorrelated and correlated media can perhaps be demonstrated more clearly by introducing a cutoff length scale ℓ for the correlations in $K(\mathbf{x})$, as described in section 2. The correlations are preserved over length scales $L < \ell$, but are lost for $L > \ell$. Naturally, the cutoff length scale ℓ must be larger than the linear size of the blocks in the computational grid. Fixing all the parameters and varying only ℓ should indicate better the effect of the correlations and their extent.

Thus, we carried out numerical simulation of acoustic wave propagation in a heterogeneous medium in which $K(\mathbf{x})$ was distributed according to an FBM with the Hurst exponent $H = 0.3$, using four cutoff lengths, $\ell = 100$, 400, 1000, and 2000 (ℓ is measured in units of $\Delta x = \Delta y$, the linear size of the blocks in the computational grid). Figure 12 presents the decay of ψ_c for the coherent wavefront. In all the cases, the ψ_c–d relation is a power law if $d < \ell$, but crosses over to an exponential function for $d \geq \ell$, in agreement with our discussions above.

Figure 13 presents the power spectrum of the waves for the four cutoff lengths. The results were computed for receivers R_{j1}, R_{j2}, R_{j3}, and R_{j4}, and then were averaged over

J. Stat. Mech. (2008) P03016

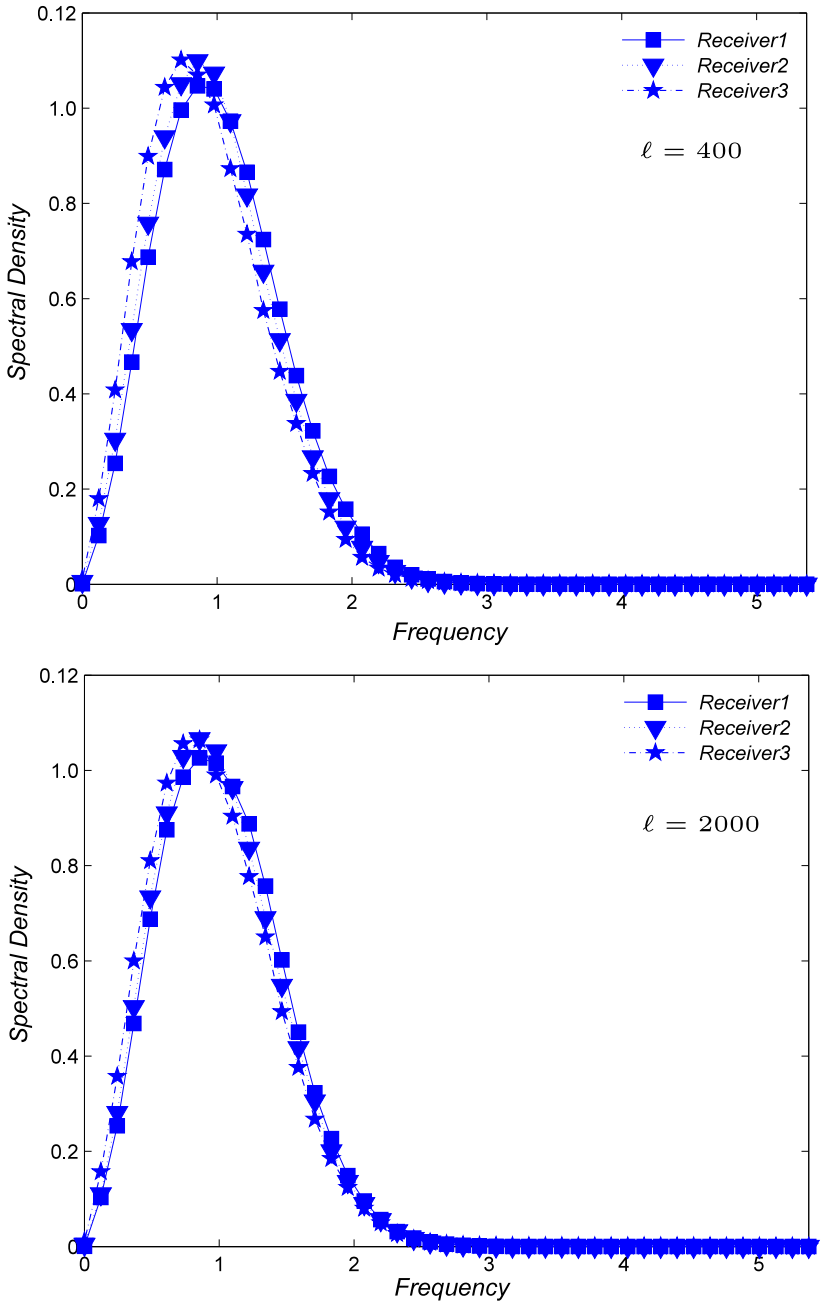

Figure 13. The normalized spectral density of the wavefront at three different receivers, as described in the text. The results are for an anisotropic medium with an FBM distribution of the local elastic constants with a Hurst exponent $H = 0.3$, and a cutoff length ℓ.

j in each case, with $j = 1$, 2, and 3. The top figure shows the spectral density for $\ell = 400$, a relatively short cutoff length. Thus, for this cutoff the medium looks like an uncorrelated one at large scales and, therefore, the spectral density is also similar to that of an uncorrelated medium shown in figure 7. By increasing ℓ, the shapes of the power spectra at different times (receivers) become increasingly similar to that of a medium with

doi:10.1088/1742-5468/2008/03/P03016

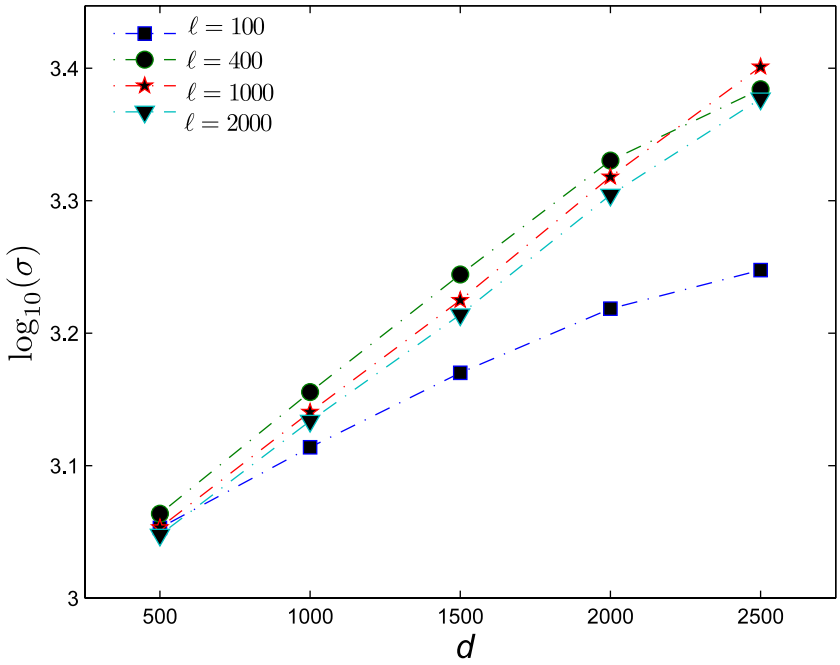

Figure 14. Dependence of the width σ of the coherent wavefront on the distance d between the source and the receivers. The medium is the same as in figure 12.

long-range correlations in the spatial distribution of its local elastic constants. Thus, there seems to be a transition from an uncorrelated to a correlated medium with long-range correlations.

Similar effects can be seen in the behavior of the width σ of the coherent wavefront. Shown in figure 14 is the dependence of σ on the source–receiver distance d for the four cases described above. For $d < \ell$ the σ–d relation is a power law, but the dependence crosses over to an exponential form for $d > \ell$.

These results also point to an important consideration in the practical applications of seismic wave propagation in heterogeneous rock, and the geophysical interpretation of the results. As shown above, the cutoff length scale ℓ—which is just the correlation length ξ for the local elastic constants—plays an important role in the transition from an uncorrelated medium to a correlated one (or between disordered media with short- and long-range correlations). At the same time, there is a relation between ξ and the range of the wavelengths that can be used in a seismic exploration of heterogeneous porous media. If ξ is smaller than the wavelength used in the exploration, the frequency dependence of the coherent wave' spectral density will be similar to that of uncorrelated media shown in figure 7. But, if the wavelength is smaller ξ, one should find a transition in the spectral density, similar to what we presented above with the various cutoff lengths ℓ. Thus, in any seismic exploration one should use a *range* of frequencies (wavelengths), in order to be able to discern the effect of the correlations in the seismic traces, and possibly detect a signature of the spatial distribution of the medium's local elastic constants. We believe that one should be able to test this proposal by careful experiments.

J. Stat. Mech. (2008) P03016

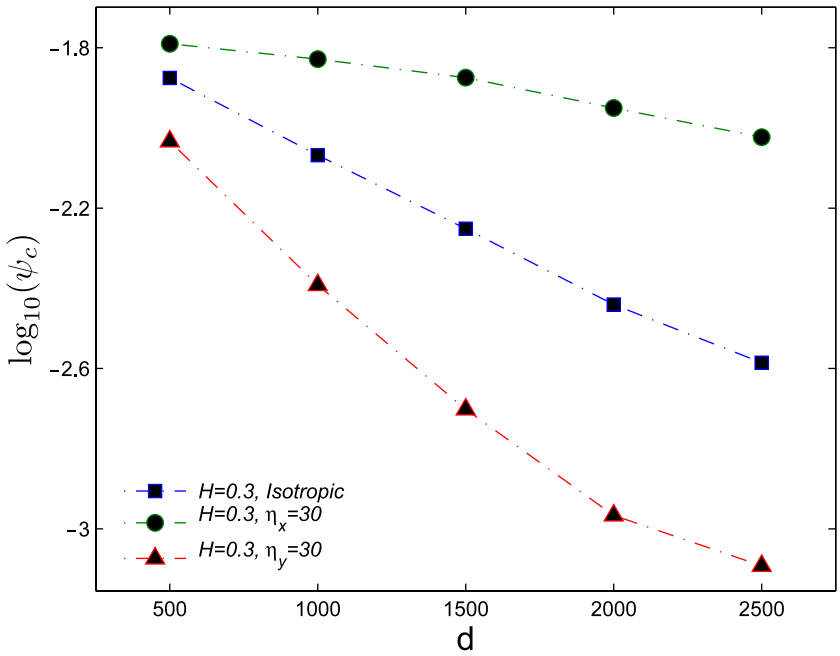

Figure 15. Dependence of the amplitude ψ_c of the coherent wavefront on the distance d between the source and the receivers, for both isotropic and anisotropic media with layers normal to the propagation direction ($\eta_x = 30$) and along the propagation direction ($\eta_y = 30$). H is the Hurst exponent.

5.3. Anisotropic media

Natural porous media, such as rock, are almost always anisotropic, with the anisotropy caused by stratification (layering). Therefore, it is important to consider the effect of anisotropy on wave propagation. We have compared acoustic wave propagation in two anisotropic media. In one case the layers are more or less parallel to the main direction y of wave propagation, indicated by $\eta_y \neq 1$ (see below), while in the second case the strata are along the x axis and normal to the main direction of the propagating waves, indicated by $\eta_x \neq 1$ (see figure 1(b)). As described in section 2, to generate the layers in a given direction, we set $\eta_i \neq 1$ ($i = x$ or y) in equation (3).

In figure 15 the decay of the quantity ψ_c of the coherent wavefront during propagation is compared for three different heterogeneous media. As the results indicate, the layers along the propagation direction have a strong effect on the amplitude decay. They essentially channelize the waves, hence leading to the sharp decay in ψ_c which is shown in the figure. In contrast, when the layers are perpendicular to the main direction of wave propagation, the amplitude decay is much slower. The behavior of ψ_c in an isotropic medium is in between.

Consistent with what we presented above in section 5.1, such distinction between the different types of heterogeneous media is also seen in the dependence of the width σ of the coherent wavefront on the source–receiver distance d; see figure 16. When the layers are parallel to the main direction of wave propagation, σ grows exponentially with d, whereas when they are perpendicular to the main direction of wave propagation, the growth of σ

J. Stat. Mech. (2008) P03016

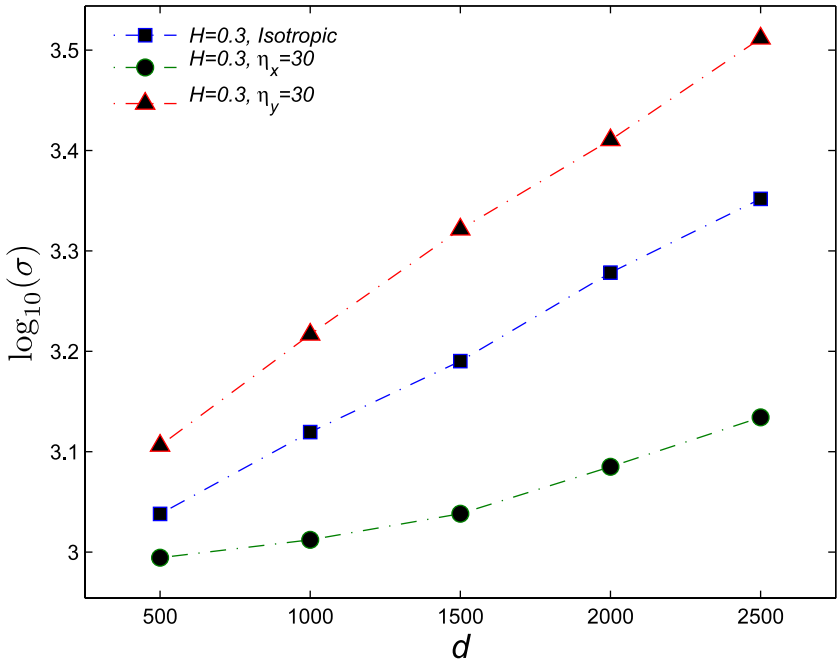

Figure 16. Same as in figure 15, but for the width σ of the coherent wavefront.

with d is much slower, similar to a linear increase. Similar to figure 15, the behavior of σ in an isotropic medium is in between.

In figure 17 the effect of the layers on the spectral density of the waves, both along the main direction of wave propagation (top figure) and perpendicular to it, is shown. In this case, however, the layers along both directions do not seem to have a strong effect on the power spectrum of the waves. In this sense, therefore, the long-range correlations (or their absence) are the most important contributing factor to the shape of the spectral density of the waves.

5.4. Dispersion relation

We have computed the dispersion relations (DRs) $\omega(k)$, by exact diagonalization of discrete wave equation for three types of 1D media: (a) a uniform system (one in which $K(x)$ is the same everywhere), (b) uncorrelated media, and (c) media with long-range correlations. Small and large values of k correspond, respectively, to long and short wavelengths. At each point of the DRs, we can compute the phase velocity, $V_{\rm p} = \omega/k$, while the slope $\mathrm{d}\omega/\mathrm{d}k$ at each point yields the group velocity $V_{\rm g}$. The computations were carried out using the exact diagonalization method [33]–[35].

We show in figure 18 the results for an uncorrelated medium, and compare them with those for a completely uniform one. For the uncorrelated medium, only for large values (short wavelengths), $k \simeq 25$, do we see deviations of the DR from that of a uniform medium (i.e., where the system starts to have dispersive behavior). This is due to the fact that, in uncorrelated media, there is much more scattering at short wavelengths than at long ones.

For the correlated media, however, the DRs are much more complex. Shown in figures 19 and 20 are the results for the Hurst exponent $H = 0.3$ and 0.8. In both cases,

J. Stat. Mech. (2008) P03016

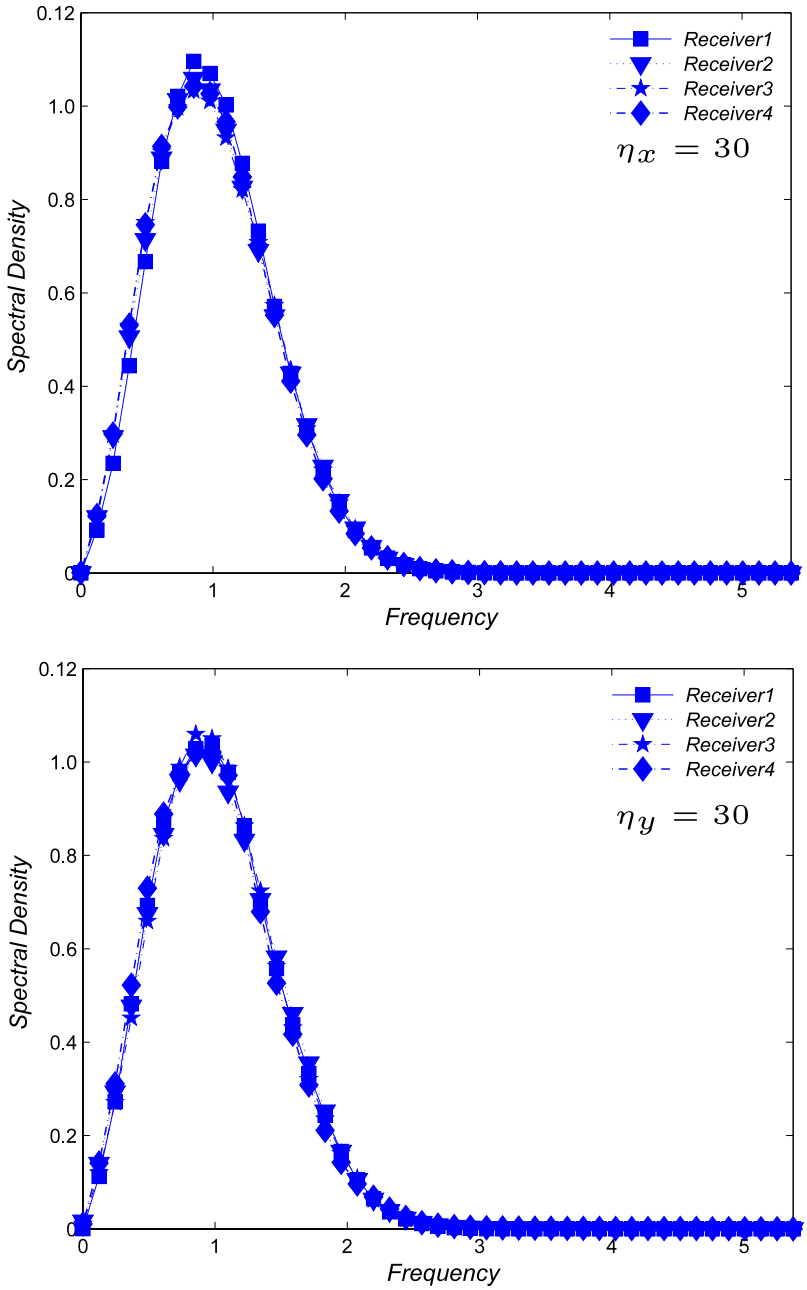

Figure 17. Normalized spectral density for the waves in anisotropic (layered) media with a Hurst exponent $H = 0.3$, when the layers are perpendicular to the main direction of wave propagation (top, $\eta_x = 30$), or are parallel to it (bottom, $\eta_y = 30$).

the deviations of the DRs for the correlated media from that of a uniform medium takes place around $k = 4\times10^{-3}$ or lower, which should be compared with that of an uncorrelated medium which happens only at short wavelengths or large k. Thus, distinct deviation of the DRs for uncorrelated and correlated media from that of a uniform medium may also be taken as another 'signature' of the existence of long-range correlations in a heterogeneous medium.

doi:10.1088/1742-5468/2008/03/P03016

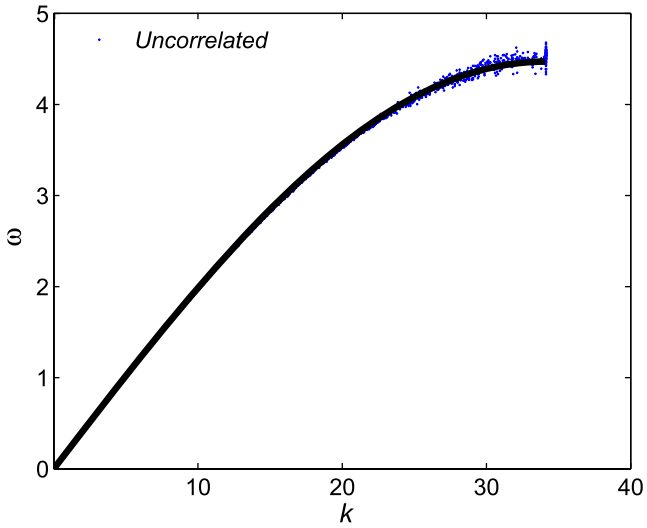

Figure 18. The dispersion relation $\omega(k)$ for an uncorrelated medium. The continuous curve shows the results for a uniform medium in which $K(\mathbf{x})$ is the same everywhere.

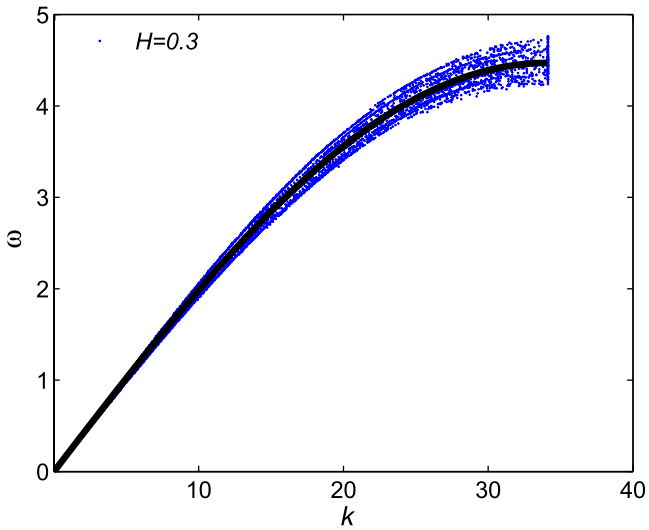

Figure 19. Same as in figure 18, but for a correlated medium with the Hurst exponent $H = 0.3$.

These results are also in agreement with what we presented above, and more specifically with those shown in figures 7 and 8. Figure 7 indicates that the ratio of low-frequency and high-frequency modes increases as the source–receiver distance d does. This indicates that, in *uncorrelated media*, the waves lose their high-frequency modes faster than the low-frequency modes, in agreement with figure 18.

On the other hand, in the correlated media, we have many phase velocities V_{p} and group velocities V_{g} for a fixed value of k. This is in agreement with the results shown in figure 8, namely, that in *correlated media* the low-frequency modes can be scattered just as efficiently and quickly as the high-frequency ones.

doi:10.1088/1742-5468/2008/03/P03016

J. Stat. Mech. (2008) P03016

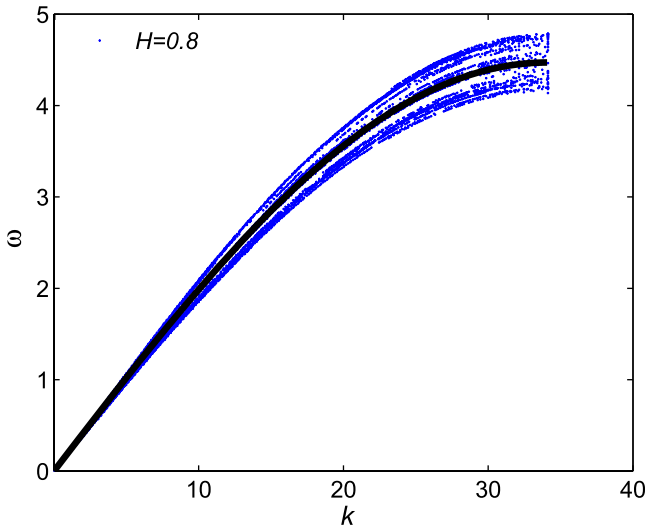

Figure 20. Same as in figure 18, but for a correlated medium with the Hurst exponent $H = 0.8$.

6. Summary

The propagation of acoustic waves in two-dimensional heterogeneous media was studied by large-scale numerical simulations. Two types of heterogeneous media were considered. One was uncorrelated media in which the local elastic constants were distributed uniformly without any correlations. Such media may also be viewed as those that contain short-range correlations, with the correlation length the limit of the resolution of the model. The second type of disordered media was characterized by spatial distributions of the local elastic constants that contained long-range correlations with power law, nondecaying correlation functions. We presented strong numerical evidence that crucial characteristics of the waves, including their amplitude decay, width, spectral density, scalogram, and the dispersion relations, are fundamentally different for uncorrelated and correlated disordered media. These aspects of wave propagation can help in the interpretation of seismic data. They can also help one to detect signatures of specific types of disorder in heterogeneous media of the type that we studied in this paper, that are abundant in nature.

Acknowledgments

The work of SMVA was supported in part by the NIOC, and the Research Council of the University of Tehran. We thank R Askari, E Pajoohesh, R Sepehrinia, and H R Siahkoohi for useful discussions.

References

[1] Torquato S, 2002 *Random Heterogeneous Materials* (New York: Springer)
[2] Sahimi M, 2003 *Heterogeneous Materials I & II* (New York: Springer)
[3] Adler P M, 1992 *Porous Media: Geometry and Transport* (Boston: Butterworth-Heinemann)
Adler P M and Thovert J-F, 1999 *Fractures and Fracture Networks* (Dordrecht: Kluwer)
[4] Sahimi M, 1993 *Rev. Mod. Phys.* **65** 1393
Sahimi M, 1995 *Flow and Transport in Porous Media and Fractured Rock* (Weinheim: VCH)

[5] Ishimaru A, 1978 *Wave Propagation and Scattering in Random Media* (New York: Academic)
Bleistein N, Cohen J K and Stockwell J W Jr, 2001 *Mathematics of Multidimensional Seismic Imaging, Migration, and Inversion* (New York: Springer)
[6] Sahimi M and Tajer S E, 2005 *Phys. Rev.* E **71** 046301
[7] Shahbazi F, Bahraminasab A, Allaei S M V, Sahimi M and Tabar M R R, 2005 *Phys. Rev. Lett.* **94** 165505
[8] Bahraminasab A, Allaei S M V, Shahbazi F, Sahimi M, Niry M D and Tabar M R R, 2007 *Phys. Rev.* B **75** 064301
[9] For recent experiments on weak localization of waves see, for example, Larose E, Margerin L, van Tiggelen B A and Campillo M, 2005 *Phys. Rev. Lett.* **93** 048501
[10] Allaei S M V and Sahimi M, 2006 *Phys. Rev. Lett.* **96** 075507
[11] Sheng P, 1995 *Introduction to Wave Scattering, Localization and Mesoscopic Phenomena* (San Diego: Academic)
[12] Older literature on the subject has been reviewed by Sornette D, 1989 *Acustica* **67** 199
Sornette D, 1989 *Acustica* **67** 251
Sornette D, 1989 *Acustica* **68** 15
[13] Carcione J M, 2001 *Wave Field in Real Media: Wave Propagation in Anisotropic, Anelastic and Porous Media* (Amsterdam: Elsevier)
[14] Kirkpatrick T R, 1985 *Phys. Rev.* B **31** 5746
Cohen S M, Machta J, Kirkpatrick T R and Condat C A, 1987 *Phys. Rev. Lett.* **58** 785
[15] Foret M, Courtens E, Vacher R and Suck J B, 1996 *Phys. Rev. Lett.* **77** 3831
Ye Z and Alvarez A, 1999 *Phys. Status Solidi* b **214** 285
Gupta B C and Ye Z, 2003 *Phys. Rev.* E **67** 036606
[16] Baluni V and Willemsen J, 1985 *Phys. Rev.* A **31** 3358
[17] Sabatier J M, Hess H, Arnott W P, Römkens M J M and Grissinger E H, 1990 *Soil Sci. Soc. Am.* **54** 68
Moore H M and Attenborough K, 1992 *Soil Sci. Soc. Am.* **43** 211
Frederickson C K, Sabatier J M and Paspet R, 1996 *J. Acoust. Soc. Am.* **99** 1326
Amédin C K, Champous Y and Berry A, 1997 *J. Acoust. Soc. Am.* **102** 1982
Hanyga A and Rok V E, 2000 *J. Acoust. Soc. Am.* **107** 2965
[18] Norris A N, 1993 *J. Acoust. Soc. Am.* **94** 359
Gurevich B and Lopatnikov S L, 1995 *Geophys. J. Int.* **121** 933
Gelinsky S and Shapiro S A, 1997 *Geophys. J. Int.* **128** F1
[19] Pride S R and Berryman J G, 2003 *Phys. Rev.* E **68** 036603
Pride S R and Berryman J G, 2003 *Phys. Rev.* E **68** 036604
Pride S R, Berryman J G and Harris J M, 2004 *J. Geophys. Res.* **109** B01201
[20] Johnson D L, 2001 *J. Acoust. Soc. Am.* **110** 682
Tserkovnyak Y and Johnson D L, 2003 *J. Acoust. Soc. Am.* **114** 2596
[21] Masson Y J, Pride S R and Nihei K T, 2006 *J. Geophys. Res.* **111** B10305
Masson Y J and Pride S R, 2007 *J. Geophys. Res.* **112** B03204
[22] Symon K R, 1960 *Mechanics* 2nd edn (Reading, MA: Addison-Wesley) p 295
[23] Flandrin P, 1989 *IEEE Trans. Inf. Theory* **35** 197
Øigård T A, Hanssen A and Scharf L L, 2006 *Phys. Rev.* E **74** 031114
[24] Flatté S M and Wu R-S, 1988 *J. Geophys. Res.* B **93** 6601
Pilkington M and Todoeschuck J, 1990 *Geophys. J. Int.* **102** 205
Klimes L, 2002 *Pure Appl. Geophys.* **159** 1811
[25] Pride S R and Masson Y J, 2006 *Phys. Rev. Lett.* **97** 184301
[26] Voss R F, 1985 *Fundamental Algorithms for Computer Graphics* (*NATO Advanced Study Institute, Series E: Applied Science* vol 17) ed R A Earnshaw (Heidelberg: Springer) p 805
[27] Pang N-N, Yu Y-K and Halpin-Healy T, 1995 *Phys. Rev.* E **52** 3224
Maske H A, Havlin S, Schwartz M and Stanley H E, 1996 *Phys. Rev.* E **53** 5445
Hamzehpour H and Sahimi M, 2006 *Phys. Rev.* E **73** 056121
[28] Dablain M A, 1986 *Geophysics* **51** 54
Kneib G and Kerner C, 1993 *Geophysics* **58** 576
[29] Somfai E, Roux J-N, Snoeijer J H, Hecke M V and van Saarloos W, 2005 *Phys. Rev.* E **72** 021301
[30] Mallat S, 1999 *A Wavelet Tour of Signal Processing* 2nd edn (London: Academic)
[31] Morlet J, Arens G, Fourgeau E and Giard D, 1982 *Geophysics* **47** 203
Morlet J, Arens G, Fourgeau E and Giard D, 1982 *Geophysics* **47** 222
[32] Kumar P and Foufoula-Georgiou E, 1997 *Rev. Geophys.* **35** 385
Sahimi M, 2000 *Annu. Rev. Comput. Phys.* **VIII** 83

J. Stat. Mech. (2008) P03016

Sahimi M, 2001 *Granular Mater.* **3** 3
Sahimi M, 2003 *Comput. Sci. Eng.* **5** 75
[33] Nussenzveig H M, 1972 *Causality and Dispersion Relations* (New York: Academic)
[34] Sachse W and Pao Y-H, 1978 *J. Appl. Phys.* **49** 4320
Weaver R L and Pao Y-H, 1981 *J. Math. Phys.* **22** 1909
[35] Sahimi M and Allaei S M V, 2008 unpublished
[36] Aström J, Kellomäki M, Alava M and Timonen J, 1997 *Phys. Rev.* E **56** 6042